

Short Communication

## Corrosion Behaviour of Low-Alloy Steel with Titanium Addition Exposed to Seawater Environment

Zhenguang Liu<sup>1</sup>, Xiuhua Gao<sup>1,\*</sup>, Linxiu Du<sup>1</sup>, Jianping Li<sup>1</sup>, Ping Li<sup>2</sup>

<sup>1</sup> The State Key Laboratory of Rolling and Automation, Northeastern University, Shenyang 110819, Liaoning, China;

<sup>2</sup> College of Chemistry, Jilin University and MacDiarmid Laboratory, Changchun 130021, Jilin, China.

\*E-mail: [liuzhenguangabcd@163.com](mailto:liuzhenguangabcd@163.com)

Received: 10 May 2016 / Accepted: 30 May 2016 / Published: 7 July 2016

---

Immersion experiment was performed to study the early seawater corrosion behaviour of pipeline steel with titanium addition by analysing microstructure characteristics of designed steel, corrosion kinetics, corrosion phases and surface morphology. The experimental results demonstrate that the microstructure of designed steel is tempered martensite and the Ti-rich particles and Cr-rich particles are observed. The corrosion rate of early seawater corrosion decreases in the exponential format. The corrosion behaviour of designed steel is divided into two stages. The Cr-rich compounds are mainly formed at the first stage and the ferrous corrosion products deposit on the coupon surface at the second stage. The main corrosion phases are goethite and lepidocrocite, and Cr-substituted goethite is also found. The titanium element accelerates the formation of the compact and dense corrosion products free of pores, which is beneficial for corrosion resistance.

---

**Keywords:** corrosion behaviour; seawater; pipeline steel; titanium; precipitation particles

### 1. INTRODUCTION

Corrosion loss in our society is enormous, and consumes more than three percent of the world's GDP[1]. Iron and steel as the structural materials are widely used in our life. Furthermore, corrosion phenomenon of iron and steel materials has attracted many scholars' attention[2,3]. In oil and gas industry, seawater corrosion is a vital practical problem for pipeline steel used in ocean environment. Notwithstanding cathodic protection and protective coating are applied on pipeline steel, corrosion is still one of the failure causes in marine environment[4]. Some experiments about carbon steel or stainless steel have clarified that corrosive electrolyte NaCl in sea water, especially Cl<sup>-</sup> ion, is the main poisonous substance for iron and steel materials[5-8]. Therefore, the research on the corrosion

behaviour of low-alloy pipeline steel used in ocean environment is necessary and pivotal given that it is inevitable for the contact of sea water and pipeline steel.

It is well accepted that the underlying corrosion performance of iron and steel materials depends on the essence of the rust layer and the chemistry-physics adhesive properties[9-11]. So, the structure and style of corrosion products play a key role on corrosion resistance. The main corrosion products in the seawater corrosion process are goethite ( $\alpha$ -FeOOH), akaganetie ( $\beta$ -FeOOH), lepidocrocite ( $\gamma$ -FeOOH) and feroxyhyte ( $\delta$ -FeOOH). The amorphous ferric oxyhydroxides also exist in the rust. The oxide compounds are hematite ( $\alpha$ -Fe<sub>2</sub>O<sub>3</sub>), maghemite ( $\gamma$ -Fe<sub>2</sub>O<sub>3</sub>), magnetite (Fe<sub>3</sub>O<sub>4</sub>) and ferrihydrite (Fe<sub>5</sub>HO<sub>8</sub>·4H<sub>2</sub>O). Those different compounds tend to be located in different positions of the rust. Ma et al[10] have observed that lepidocrocite and goethite are prior to be in the outer layer, and akaganetie is formed in the inner layer. Magnetite is only located in the outer layer. On the contrary, maghemite is solely observed in the inner layer. The amorphous corrosion products are distributed in both the inner layer and outer layer. For the design of anti-corrosion steel, alloying elements, such as chromium, nickel, copper and phosphorus, are usually added to the steel substrate with low cost to promote the corrosion resistance greatly. Alloying elements are not responsible for the appearance of different corrosion products on the steel surface, and alloying elements influence the corrosion products' proportion and degree of crystallinity[11]. Chromium is a normal element used to form the stable and protective rust layer. The amorphous ferric oxyhydroxide FeO<sub>x</sub>(OH)<sub>3-2x</sub> or Cr-substituted goethite are observed in the inner layer[12-14], and the compact layer free of cracks could preclude the permeation of corrosion ions in the electrolyte solution. The anode and cathode reactions are also inhibited consequently. For the early corrosion behaviour of steel materials, Melchers et al[15] have investigated the early corrosion behaviour of mild steel in seawater environment. They point out that the seawater corrosion behaviour is initially highly non-linear and then almost linear until the formation process of corrosion products begins to control the corrosion rate. Furthermore, the corrosion process of steel materials with long-term corrosion time could be divided into two stages, and the corrosion rate of the first stage is higher than that of the second stage[9,16-18]. Melchers[19,20] has also pointed out that corrosion loss behaviour bases on the oxygen diffusion characterised with a series of sequential phases. For the corrosion mechanism, Morcillo et al[21] summarises the rusting formation mechanism and the protective property of weathering steel. It is accepted that those precious data and knowledge are valuable to design and study the new pipeline steel used in ocean environment with novel corrosion resistance. For the design of low-alloy pipeline steel, the titanium element usually is widely used to add into the steel substrate to improve the mechanical strength through the effect of precipitation strength[22-24]. The role of titanium element on the seawater corrosion behaviour is seldom reported.

According to other researchers' investigation mentioned above, their attentions focus on the corrosion behaviour of carbon steel exposed to marine or atmospheric environment. The investigation on the corrosion behaviour of low-alloy pipeline steel exposed to seawater environment is rare, and the early corrosion behaviour and mechanism is seldom reported. In addition, there are few literatures about the role of titanium element on the seawater corrosion behaviour though the titanium is widely used in the low-alloy steel. In this paper, the immersion experiment is carried out to study the seawater corrosion behaviour of low-alloy pipeline steel with titanium addition by analysing microstructure of

designed steel, macroscopic/microscopic surface morphology, energy dispersive X-ray diffraction (EDX) spectrum, XRD and corrosion kinetic curves. The role of chromium and titanium elements on the formation of corrosion products is also investigated. The corrosion behaviour and mechanism of designed steel is discussed according to the experimental results.

## 2. MATERIAL AND EXPERIMENT

### 2.1 Material and experimental process

The designed steel with the chemical compositions (mass.%): C 0.07, Si 0.24, Mn 0.81, P 0.003, S 0.0018, Cr 1.0 (max), Mo 0.5 (max), Al 0.04, Ti 0.06, Fe balance, was melted with a vacuum furnace followed by casting into ingot. Then, the ingot was hot rolled into the thick plate from 80 mm to 10 mm, and the cold rolling process was also carried out to fabricate the final experimental material with the thickness of 4 mm. The heat treatment process of quenching and tempering (quenching temperature 900 °C + dwell time 15 minutes and tempering temperature 350 °C + dwell time 30 minutes) was utilized to improve the microstructure and mechanical property, which is crucial to the pipeline steel. Prior to experiment, the coupons with the dimension of 50 mm × 25 mm × 4 mm were polished by using 240 #, 400 # and 600 # silicon carbide papers, respectively. Then, those coupons were cleaned ultrasonically in alcohol, dried with cold air. Those coupons are weighted originally with a balance with the precision of 0.01mg and stored in a desiccator free of moisture.

Immersion experiment was utilized to simulate the corrosion process of pipeline steel exposed to seawater environment. The electrolyte solution was 3.5 mass% NaCl, and the experimental temperature was 25 °C. The immersion durations chosen in this experiment were 24 h, 48 h, 72 h, 120 h, 192 h, 360 h and 600 h. Three replicate coupons were used in the individual immersion duration. The chemical cleaning method was adopted to descale the corrosion products on the coupons surface. The chemical compositions of etching solution were 500 mL 37vol% hydrochloric acid, 500 mL distilled water and 20 g hexamethy lenetebamine (urotropine). The function of hexamethy lenetebamine was to suppress effectively the chemical dissolution of steel substrate in the process of removing corrosion rust[25]. Those cleaned coupons were weighted again to calculate the mass loss. The corrosion rate ( $CR$ ,  $\text{mm}\cdot\text{y}^{-1}$ ) was determined using the following equation based on the standard of ASTM G1-03[26]:

$$CR = \frac{87,600\Delta m}{t\rho S} \quad (1)$$

where  $\Delta m$  is the mass loss, g;  $t$  is the immersion time, h;  $\rho$  is the physical density of designed steel,  $\text{g}\cdot\text{cm}^{-3}$ ;  $S$  is the coupon surface area,  $\text{cm}^2$ .

### 2.2 Morphology observation and analysis

The macroscopic and microscopic surface morphology of corroded coupons was characterised by using FEI QUANTA 600 scanning electron microscopy (SEM). Energy dispersive X-ray (EDX)

was also used to analyse the chemical compositions of surface rust. X-ray diffraction (XRD) with  $\text{Co}_{K\alpha}$  radiation and a step of  $0.04^\circ$  was carried out to study the corrosion products. The styles of corrosion phases were detected by matching the position of characteristic peaks automatically with MDI Jade software equipped with database PDF-2(2004). The microstructure of designed steel was obtained by using LEICA DMIRM optical microscope (OM) and ZEISS ULTRA55 field emission scanning electron microscopy (FE-SEM). Furthermore, FEI Tecnai G<sup>2</sup>F20 transmission electron microscope (TEM) equipped with EDX was used to show the microstructure morphology in detail and the chemical compositions of the precipitate particles in the designed steel.

### 3. RESULTS AND DISCUSSION

#### 3.1 Microstructure morphology

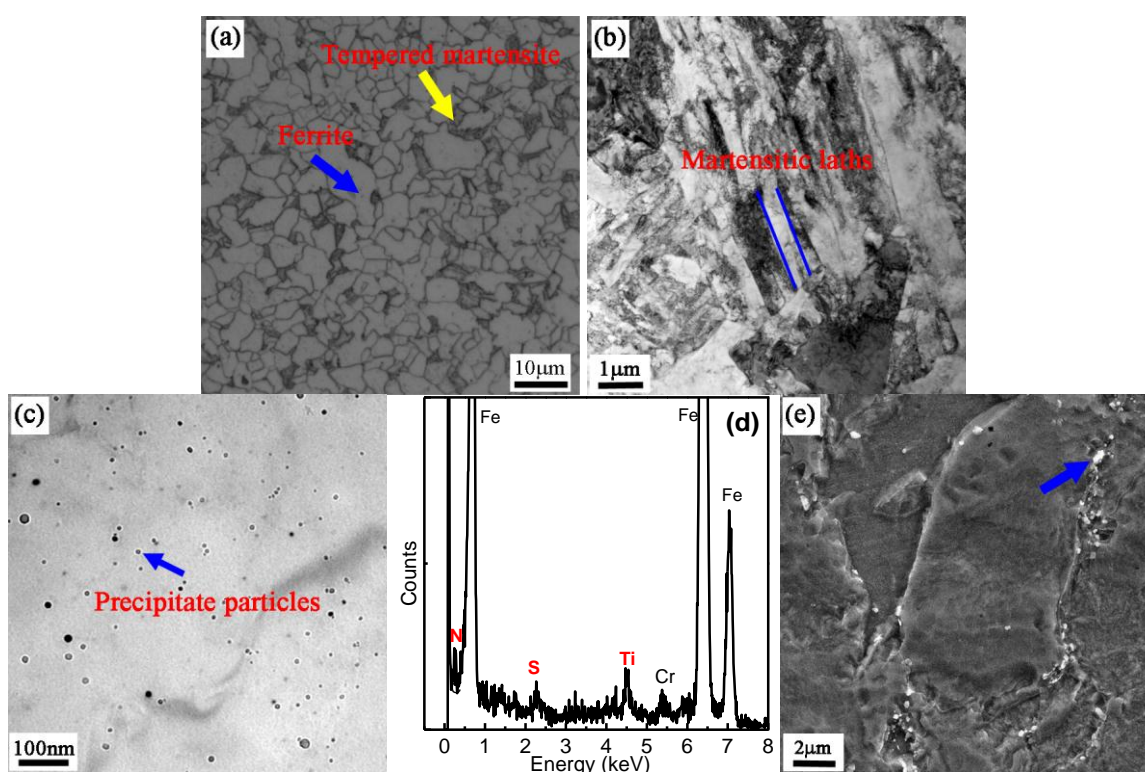


**Figure 1.** Microstructure morphology of designed steel: (a) OM; (b) TEM; (c) TEM-precipitate particles; (d) EDX result of the special particle marked with blue arrow in Figure 1c; (e) FE-SEM.

The metallurgical microstructure morphology is revealed by using OM, FE-SEM and TEM. Fig. 1a shows that the microstructure of designed steel consists of ferrite and tempered martensite. Transmission electron microscope is used to further reveal the microstructure morphology. Fig. 1b shows that the martensitic laths are observed. Therefore, it is confirmed that the microstructure comprises ferrite and tempered martensite. In this experiment, titanium element is added to the

designed steel to obtain high mechanical strength through the effect of precipitation strength. Fig. 1c shows that the random precipitate particles are found in the designed steel. The result of EDX analysis (Fig. 1d) demonstrates that those particles marked with blue arrow in Fig. 1c contain titanium element. Based on the morphology characteristics, they are Ti(C,N) particles. Fig. 1e shows that many particles are observed in the grain inside and grain boundary. The EDX analysis demonstrates that those particles contain chromium element, and they are Cr-rich carbides. Other researchers' investigation proves that the initiation of corrosion process nucleates in the ferritic matrix near cementite nodes[21]. Therefore, the microstructure characteristics in the designed steel may influence the seawater corrosion behaviour, which will be discussed in the following section.

### 3.2 Corrosion kinetics

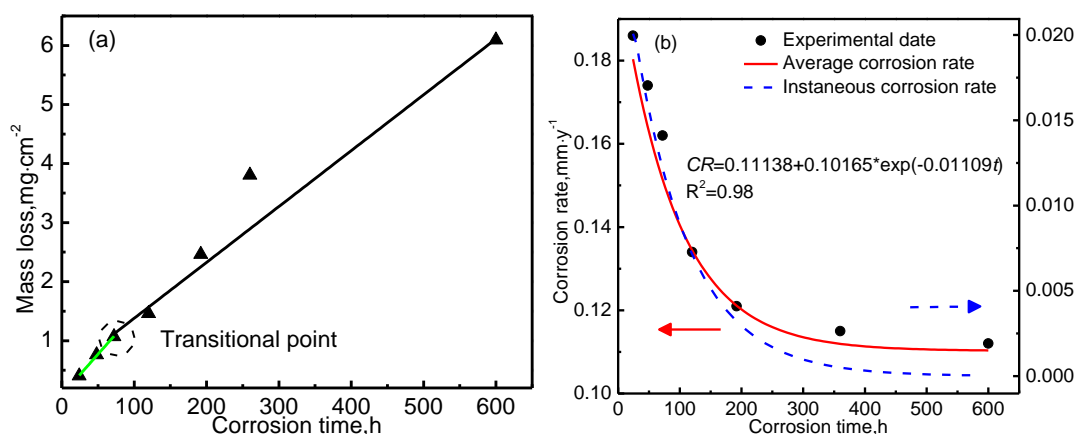


**Figure 2.** Corrosion kinetic curves: (a) mass loss; (b) corrosion rate.

For corrosion process, the kinetic curves of mass loss and corrosion rate generally reflect the corrosion behaviour. Fig. 2 lists the corrosion kinetic curves of designed steel. The values shown in the figures are the average for three duplicated coupons immersed in the individual immersion duration. Fig. 2a reveals that the early seawater corrosion behaviour of designed steel is divided into two stages according to the curve of mass loss. The slope of the first stage (24 h-72 h) is higher than that of the second stage (120 h-600 h). That case indicates that the corrosion process of the first stage is faster than that of the second stage. Similarly, Fig. 2b shows that the corrosion rate of the first stage is higher than that of the second stage. The corrosion rate decreases sharply at the first stage. Furthermore, the experimental data indicate that the relationship of immersion time and corrosion rate fits the function format:  $y = y_0 + A \cdot \exp R_0 \cdot x$ . So, the fitting function (solid red line) with  $R^2 = 0.98$  (equation 2) is proposed based on the experimental data. The fitting curve of corrosion rate demonstrates that the corrosion rate of designed steel meets the exponential format. For corrosion process of steel materials, the instantaneous corrosion rate explains the changing trend of corrosion rate. The curve of instantaneous corrosion rate (dotted blue line) is plotted according to the fitting function. Those curves show that both actual corrosion rate and instantaneous corrosion rate decrease versus corrosion time. That case indicates that the corrosion process is precluded with increasing corrosion time.

Furthermore, the corrosion rate decreases sharply at the first stage and moderately at the second stage. Therefore, the chemical reaction rate of the first stage is higher than that of the second stage.

$$CR = 0.11138 + 0.10165 \cdot \exp(-0.01109t) \quad (2)$$

where  $CR$  is corrosion rate,  $\text{mm} \cdot \text{y}^{-1}$ ,  $t$  is corrosion time, h.

### 3.3 Corrosion phases

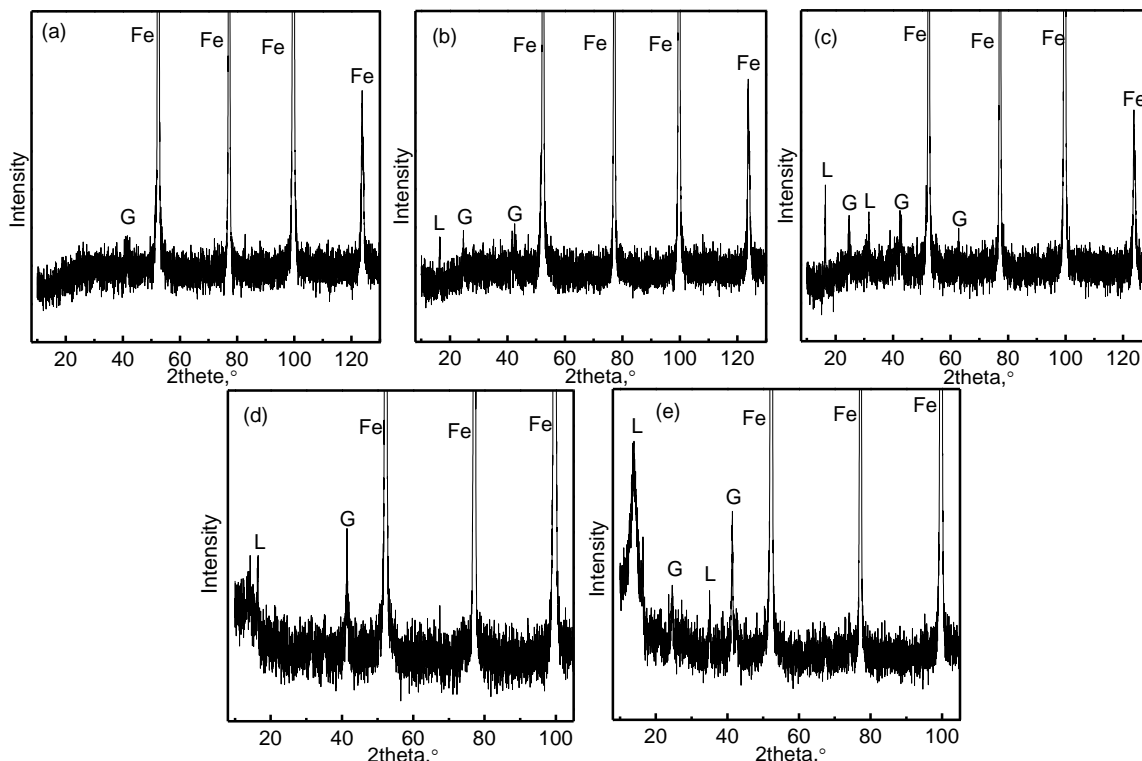


**Figure 3.** XRD pattern for different immersion durations: (a) 72 h; (b) 120 h; (c) 192 h; (d) 360 h; (e) 600 h. L-lepidocrocite, G-goethite.

The corrosion behaviour of steel materials is related to the corrosion products[9-12]. Fig. 3 lists the XRD pattern of corrosion phases on the coupon surface of individual immersion duration. The corrosion products are not detected on the coupon surface of 24 h and 48 h immersion durations. So, the XRD pattern is not showed. According to the experimental results, the main corrosion products are lepidocrocite and goethite. At the initial stage (Fig. 3a), only goethite is found. With prolonging immersion time, corrosion products transform into goethite and lepidocrocite (Fig. 3b-e). The steel substrate is also detected on the coupon surface, demonstrating that the corrosion products may easily be dropped from the steel substrate.

### 3.4 Macroscopic morphology

Fig. 4 shows the macroscopic surface morphology of the designed steel after different immersion durations. Fig. 4a shows that the coupon surface of 24 h immersion is partially covered

with the corrosion products and the polished scratch marked with blue arrow is still observed. That phenomenon demonstrates that the corrosion process is at the beginning stage and the corrosion products are formed locally on the coupon surface.

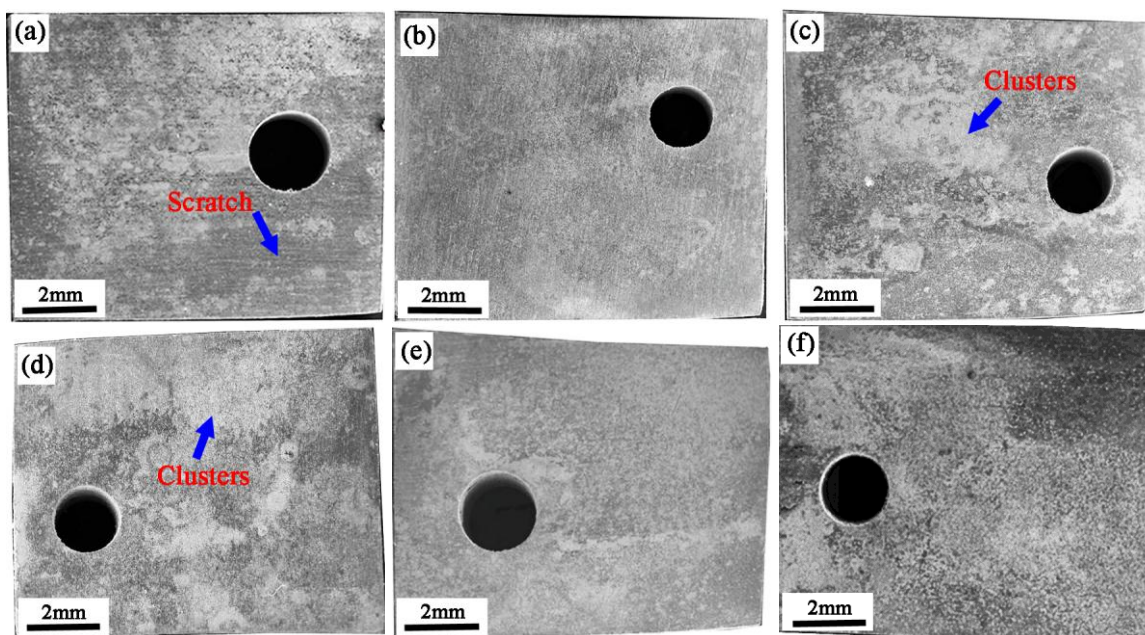


**Figure 4.** Macroscopic surface morphology for different immersion durations: (a) 24 h; (b) 72 h; (c) 120 h; (d) 192 h; (e) 360 h; (f) 600 h.

With increasing immersion time, the coupon surface of 72 h immersion is wholly covered with corrosion products (Fig. 4b). That case indicates that the primary corrosion rust appears on the coupon surface. That layer prevents the oxygen and chloride elements in the electrolyte solution from accessing into the steel substrate. So, the increment of mass loss increases slowly after 72 h immersion (Fig. 2a) and the corrosion rate also decrease fast after that time (Fig. 2b). With prolonging corrosion time, the coupon surface is stacked with corrosion products in clusters (Fig. 4c and d) and the compact layer is formed after long immersion time (Fig. 4e and f). Moreover, the structure of corrosion products becomes more compact and denser, leading to the excellent corrosion resistance. Therefore, the corrosion rate is lower after 72 h immersion.

### 3.5 Microscopic morphology

The essence of corrosion resistance is that the solid and thick layer is formed on the coupon surface[27,28]. That layer acts as a barrier to prevent the corrosion ions in the electrolyte solution accessing into the interface of steel substrate and corrosion products. The microscopic morphology of corrosion products for different immersion durations is listed in Fig. 5. At the first stage, the corrosion products are not formed on the coupon surface of 24 h immersion, and some crackings are observed (the inset in Fig. 5a). Those crackings provide the access channel of the corrosion ion, such as oxygen and chlorine. Therefore, the corrosion resistance is poor and the corrosion rate is high (Fig. 2b). The

EDX analysis shows that the corrosion products on the coupon surface of 24 h immersion (Fig. 5a) is rich in chromium element.

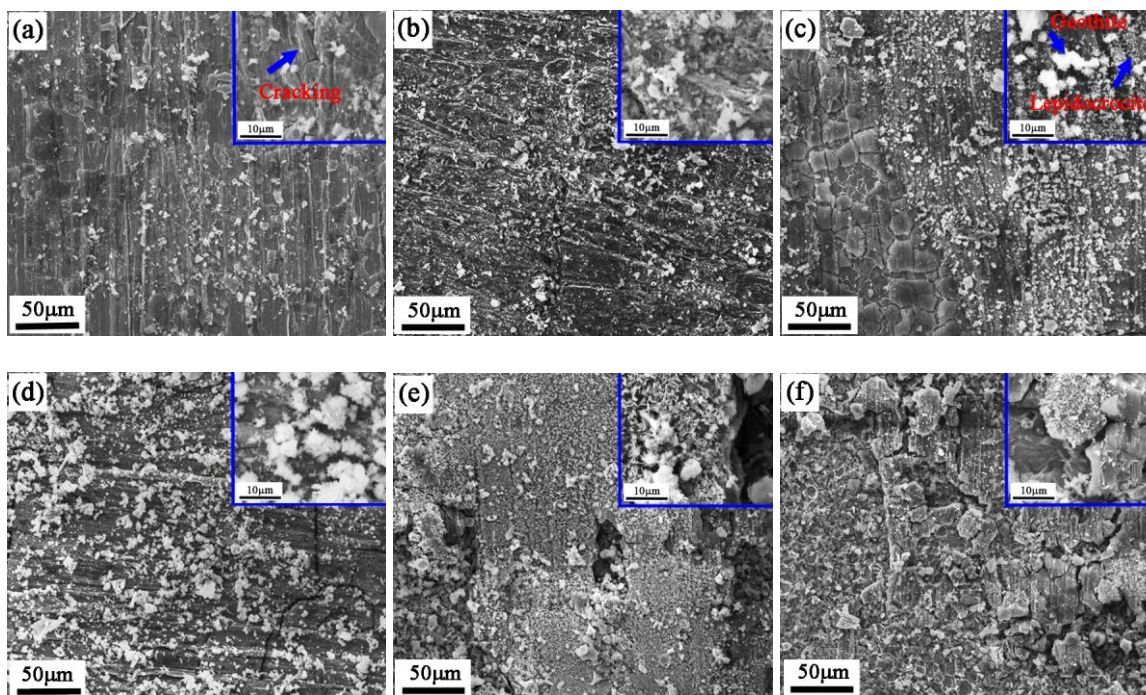
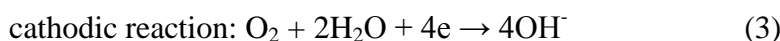
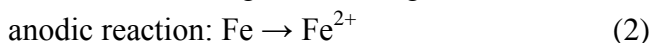


**Figure 5.** Microscopic surface morphology for different immersion durations: (a) 24 h; (b) 72 h ; (c) 120 h; (d) 192 h; (e) 360 h; (f) 600 h.

Therefore, the corrosion products are Cr-rich compounds. As the Cr-rich compounds are in the amorphous formation, they are not detected by the XRD. In this experiment, chromium element is added into the steel substrate to improve corrosion resistance. Chromium element is passivity promoter as it combines low metal-metal bond strength with high metal-oxygen bond strength. The low metal-metal bond strength is important for the rapid nucleation and growth of the oxides by facilitating the breaking of the surface metal-metal bonds in the early stages of passivation[29]. So, the Cr-rich compounds are prior to be formed on the coupon surface. Fig. 5a demonstrates that at the first stage, the main corrosion process is the formation of Cr-rich compounds and the ferrous corrosion products are not found. The thin corrosion rust layer formed at the first stage. That rust acts the shield between the steel substrate and electrolyte solution to protect the steel substrate. Therefore, the corrosion rate decreases fast at the first stage (Fig. 2b). For the second stage, small particles of corrosion products are accumulated on the coupon surface of 72 h immersion (Fig. 5b). Fig. 5c shows that the corrosion products with cotton ball shape structure and flowery structure (the inset in Fig. 5c) are formed, which are goethite and lepidocrocite, respectively[9,10,18]. The surface morphology is agreed with the XRD result (Fig. 3b). However, some crackings are still exhibited on the coupon surface. With increasing corrosion time, the coupon surface of 192 h immersion (Fig. 5d) is covered with geothite, and the size of goethite is bigger than that of 120 h immersion (Fig. 5c). The distribution of goethite crystals is dispersed and the large crackings are still revealed on the coupon surface. That surface characteristics demonstrate that the corrosion ions in electrolyte solution could still react with the steel substrate. The

dense and compact layer is formed on the coupon surface of 360 h immersion (Fig. 5e), and the corrosion products are also goethite and lepidocrocite. That solid rust prevents the contact of steel substrate and corrosion ions and improves the passivation capability of designed steel. So, the anodic and cathodic reactions described by reaction (2)-(4)[10,30] are also suppressed. After 600 h immersion (Fig. 5f), corrosion products become stiff and the rust layer is thicker. Therefore, the corrosion rate decreases due to this denser and thicker rust. Fig. 5b-Fig. 5f show that at the second stage, the main corrosion process is the formation of ferrous corrosion products. As the thin corrosion film is formed at the first stage, the diffusion or exchange of the corrosion ions and steel substrate is inhibited. At the second stage, the formation process of corrosion products may be slow. The consumption of steel substrate decreases with prolonging corrosion time. Therefore, the corrosion rate of second stage is lower than that of first stage. The change of corrosion rate of the second stage is small (Fig. 2b).



### 3.6 The effect of chromium and titanium elements on corrosion products

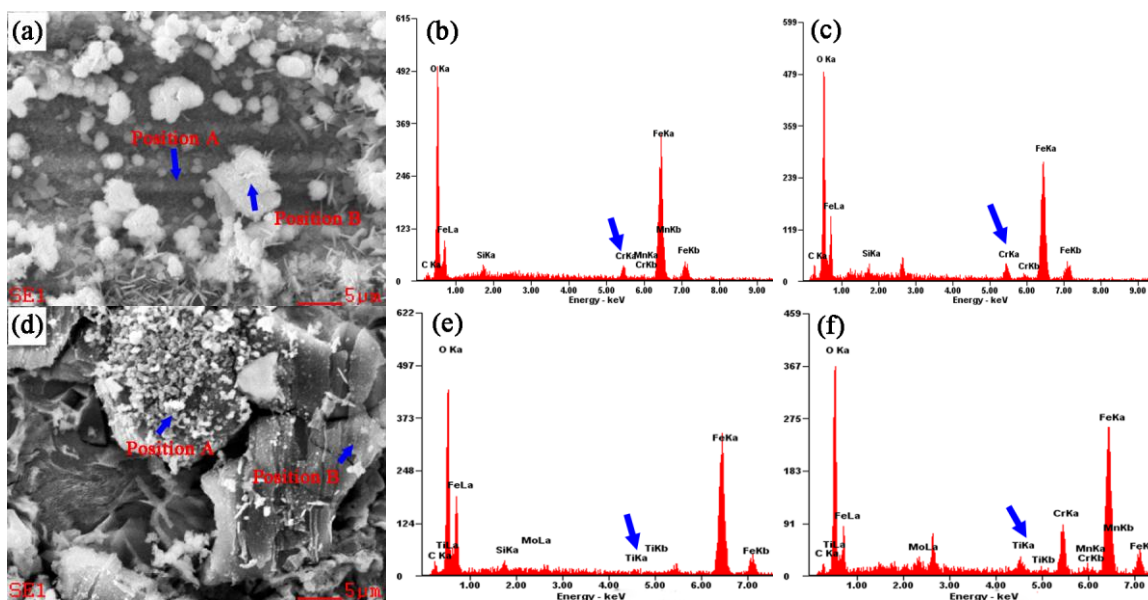


**Figure 6.** EDX analysis of the corrosion products on the coupon surface: (a) Cr-rich corrosion products and EDX results (b) and (c), corresponding to position A and B in Figure 6a, respectively; (d) Ti-rich corrosion products and EDX results (e) and (f), corresponding to position A and B in Figure 6d, respectively.

For the design of anti-corrosion steel, it is an effective and economic solution to add chromium element to steel substrate to improve corrosion resistance. Some researchers' investigations show that chromium element accumulates in the inner layer and gives rise to the formation of nonphase goethite, identified as Cr-substituted goethite,  $\alpha\text{-(Fe}_{1-x}\text{Cr}_x)\text{OOH}$  or  $\text{Fe}_x\text{Cr}_{1-x}\text{OOH}$ [12-14,30]. In this experiment, the chemical compositions of corrosion products on the coupon surface of 600 h

immersion are detected by using EDX spectrum. The results demonstrate that both the corrosion products of the inner layer (position A in Fig. 6a) and the corrosion products of outer layer (position B in Fig. 6a) consist of chromium element (Fig. 6b and c, respectively). According to the surface morphology, the corrosion products of position A in Fig. 6a is the Cr-rich compound, which is formed at the first stage, and the corrosion product of position B in Fig. 6a with cotton ball structure is Cr-substituted goethite, which is formed at the second stage. That phenomenon shows that chromium element in the steel substrate promotes the formation of amorphous ferroxidate through the catalytic effect. Chromium element could dissolve into the steel substrate with the large solubility. When the steel substrate changes into corrosion products, chromium element in the steel substrate is redistributed owing to the solubility distinction between corrosion products and steel substrate. Chromium element in the steel substrate replaces the iron element in the iron oxyhydroxide to form Cr-substituted goethite[13]. In addition, Cr-rich carbides are observed in the steel substrate showed in Fig. 1e. Those Cr-rich carbides in the steel substrate may act as the embryo for the nucleation and growth of crystal goethite[31]. So, the Cr-substituted goethite is formed. In general, the roles of chromium element are two effects. The one is that it changes into the Cr-rich compounds at the first stage. The other is that it may replace the iron atom and form the Cr-substituted goethite. Titanium element is the fascinating element to improve the mechanical strength due to the precipitate particles and may also influence the corrosion behaviour. Ti-rich precipitate particles are observed in the microstructure of designed steel (Fig. 1c). EDX analysis demonstrates that both the fine corrosion product (position A in Fig. 6d) and the solid corrosion products (position B in Fig. 6d) are rich in titanium element (Fig. 6e and f, respectively). Those titanium-containing corrosion products are extremely dense and free of pores and crackings, which is beneficial for the corrosion resistance. Other investigations show that the addition of titanium element increases the crystallite size of goethite and produces double domain particles consisting of the particles core and porous crystallite shell[32]. In our research, the experimental results demonstrate that the titanium element also promotes the formation of compact and dense corrosion products. That structure is beneficial for corrosion resistance. Furthermore, Ti-rich precipitate particles may change the nucleation style of corrosion products from the homogeneous nucleation through prenucleation embryo to heterogeneous nucleation through the precipitate particles[33]. So, the titanium-containing rust on the coupon surface is the effective and stable protective layer. That structure acts as the wall to protect the steel substrate.

#### 4. CONCLUSIONS

The immersion experiment was carried out to study the seawater corrosion behaviour of pipeline steel used in ocean environment by investigating the microstructure of designed steel, corrosion kinetics, corrosion phases, macroscopic/microscopic surface morphology. In addition, the role of chromium and titanium elements on the formation of corrosion products is also studied. According to the experimental results, some conclusions are summarised in following.

(1) The microstructure of designed steel consists of tempered martensite, the Ti-rich precipitate particles and Cr-rich particles are observed in the steel substrate.

(2) The corrosion rate of the early corrosion stage follows the exponential format. The corrosion behaviour of designed steel is divided into two stages. At the first stage, the main corrosion process is the formation of Cr-rich compounds. While, at the second stage, the one is the formation of ferrous corrosion product. The main corrosion phases are goethite and lepidocrocite. Meantime, Cr-substituted goethite is observed on the coupon surface.

(3) The chromium element changes into the Cr-rich compounds or replaces the iron atom in the corrosion products of goethite. Titanium element promotes the formation of compact and dense rust free of pores.

#### ACKNOWLEDGEMENT

The authors are grateful for financial support from National High Technology Research and Development Program of China (2015AA03A501) and Natural Science Foundation of China (NSFC, 51274063).

#### References

1. F. U. Renner, A. Stierle, H. Dosch, *Nature*, 439(2006) 707.
2. H.W. Wang, P. Zhou, S.W. Huang, C. Yu, *Int. J. Electrochem. Sci.*, 11 (2016) 1293.
3. K.F. Khaled, A. M El-Sherik, *Int. J. Electrochem. Sci.*, 11 (2016) 2377.
4. I. A. Chaves, R. E. Melchers, *Corros. Sci.*, 53(2011) 4026.
5. Q. Hu, Y. B. Qiu, X. P. Guo, J. Y. Huang, *Corros. Sci.*, 52(2010) 1205-1212.
6. R. E. Melchers, *Corros. Sci.*, 46(2004) 1669.
7. Y. Ait Albrimi, A. Ait Addi, J. Douch, M. Hamdani, R.M. Souto, *Int. J. Electrochem. Sci.*, 11 (2016) 385.
8. Q. Hu, G. A. Zhang, Y. B. Qiu, X. P. Guo, *Corros. Sci.*, 53(2011) 4065.
9. X.M. Ma, B. Qian, J. Zhang, W.C. Xu, Q.T. Jiang, M. Zheng, F.B. Ma, B.R. Hou, *Int. J. Electrochem. Sci.*, 11 (2016) 3024.
10. Y. T. Ma, Y. Li, F. H. Wang, *Mater. Chem. Phys.*, 112(2008) 844.
11. J. G. Castaño, C. A. Restrepo, E. A. Agudelo, E. Correa, F. Echeverría, *Corros. Sci.*, 52(2010) 216.
12. I. Diaz, H. Cano, D. Fuente, B. Chico, J. M. Vega, M. Morcillo, *Corros. Sci.*, 76(2013) 348.
13. Q. C. Zhang, J. S. Wu, J. J. Wang, W. L. Zheng, J. G. Chen, A. B. Li, *Mater. Chem. Phys.*, 77(2002) 603.
14. H. Canoe, D. Neff, M. Morcillo, P. Dillmann, I. Diaz, D. Fuente, *Corros. Sci.*, 87(2014) 438.
15. R. E. Melchers, R. Jeffrey, *Corros. Sci.*, 47(2005) 1678.
16. L. Hao, S. X. Zhang, J. H Dong, W. Ke, *Corros. Sci.*, 53(2011) 4187.
17. Y. T. Ma, H. Li, F. H. Wang, *Corros. Sci.*, 52(2010) 1796.
18. Y. T. Ma, H. Li, F. H. Wang, *Corros. Sci.*, 51(2009) 997.
19. R. E. Melchers, *Corros. Sci.*, 68(2013) 186.
20. R. E. Melchers, *Corros. Sci.*, 50(2008) 3446.
21. M. Morcillo, I. Díaz, B. Chico, H.Cano, D. Fuente, *Corros. Sci.*, 83(2014) 6.
22. Z. W. Peng, L. J. Li, J. X. Gao, X. D. Huo, *Mater. Sci. Eng. A-Struce.*, 657(2016) 413.
23. Y. L. Kang, Q. H. Han, X. M. Zhao, M. H. Cai, *Mater. Design.*, 44(2013) 331.
24. S. Mukherjee, I. B. Timokhina, C. Zhu, S. P. Ringer, P.D. Hodgson, *Acta. Mater.*, 61(2013) 2521.
25. Y.H. Qian, C.H. Ma, D. Niu, J.J. Xu, M.S. Li, *Corros. Sci.*, 74(2013) 424.
26. ASTM G1-03, ASTM International, West Conshohocken, 2011.
27. Y. Zhou, Y. Zuo, *Appl. Surf. Sci.*, 353(2015) 924.

28. Y. F. Wang, G. X. Cheng, W. Wu, Q. Qiao, Y. Li, X. F. Li, *Appl. Surf. Sci.*, 349(2015) 746.
29. O. Yevtushenko, D. Bettge, S. Bohraus, R. Bäbler, A. Pfennig, A. Kranzmann, *Process. Saf. Environ.*, 92(2014) 108.
30. Y. H Qian, C. H. Ma, D. Niu, J. J Xu, M. S. Li, *Corros. Sci.*, 74(2013) 424.
31. J. D. Yoreo, *Nature. Mater.*, 12(2013) 284.
32. T. Nakayama, T. Ishikawa, T. J. Konno, *Corros. Sci.*, 47(2005) 2521.
33. Z. G. Liu, X. H. Gao, Y. Chi, L. X. Du, J. P. Li, P. J. Hao, *Acta. Metall. Sin. (Engl. Lett.)*, 28(2015) 739.

© 2016 The Authors. Published by ESG ([www.electrochemsci.org](http://www.electrochemsci.org)). This article is an open access article distributed under the terms and conditions of the Creative Commons Attribution license (<http://creativecommons.org/licenses/by/4.0/>).